Nanoscopy using a semiconductor heterostructure as the sample stage

Hasan Tahir Abbas,[1,2] Xiaodong Zeng,[3,*] Robert D. Nevels,[1,*] and M. Suhail Zubairy [1]

[1] *Department of Electrical and Computer Engineering, Texas A&M University, College Station, TX 77843 USA*
[2] *University of Engineering & Technology Lahore (KSK) 54890, Pakistan*
[3] *Institute for Quantum Science and Engineering (IQSE) and Department of Physics and Astronomy, Texas A & M University, College Station, Texas 77843-4242, USA*
[*] *opex@osa.org*

Abstract: A special structured illumination microscopy scheme using a two dimensional electron gas as the sample stage is proposed. Terahertz plasma waves generated by a current-driven instability illuminate the sample. Concurrently, a plane wave is used to shift the plasmonic pattern needed to expand the observable range of spatial frequencies. Full coverage of the spatial frequency regime is obtained by tuning the plasma waves through gate voltage control. Hence, it is possible to reconstruct an image with resolution up to two orders of magnitude beyond the diffraction limit. Due to the linear nature of the technique, only a weak illumination signal is required, therefore minimizing the likelihood of sample damage due to radiation.

OCIS codes: (100.0100) Image processing; (180.0180) Microscopy; (270.0270) Quantum optics; (050.6624) Subwavelength structures; (110.6795) Terahertz imaging; (120.4120) Moire' techniques; (130.5990) Semiconductors; (240.6680) Surface plasmons; (100.6640) Superresolution; (240.6690) Surface waves.

References and links

1. M. Minsky, "Memoir on inventing the confocal scanning microscope," Scanning **10**, 128–138 (1988).
2. M. G. L. Gustafsson, "Surpassing the lateral resolution limit by a factor of two using structured illumination microscopy." J. Microsc. **198**, 82–87 (2000).
3. R. Heintzmann and C. G. Cremer, "Laterally modulated excitation microscopy: Improvement of resolution by using a diffraction grating," in "Optical Biopsies and Microscopic Techniques III," , vol. 3568 I. J. Bigio, H. Schneckenburger, J. Slavik, K. Svanberg, and P. M. Viallet, eds. (SPIE, 1999), vol. 3568, pp. 185–196.
4. R. Heintzmann and G. Ficz, "Breaking the resolution limit in light microscopy," Brief. Funct. Genomic. Proteomic. **5**, 289–301 (2006).
5. M. G. L. Gustafsson, "Nonlinear structured-illumination microscopy: Wide-field fluorescence imaging with theoretically unlimited resolution," Proc. Natl. Acad. Sci. U.S.A. **102**, 13081–13086 (2005).
6. H. Nassenstein, "Superresolution by diffraction of subwaves," Opt. Commun. **2**, 231–234 (1970).
7. F. Wei and Z. Liu, "Plasmonic structured illumination microscopy," Nano Lett. **10**, 2531–2536 (2010).
8. X. Zeng, M. Al-Amri, and M. S. Zubairy, "Nanometer-scale microscopy via graphene plasmons," Phys. Rev. B **90**, 2–6 (2014).
9. X. Zeng, L. Fan, and M. S. Zubairy, "Deep-subwavelength lithography via graphene plasmons," Phys. Rev. A **95** (2017).
10. A. B. Mikhailovskii, *Theory of Plasma Instabilities* (Springer, 2013).
11. K. Kempa, P. Bakshi, J. Cen, and H. Xie, "Spontaneous generation of plasmons by ballistic electrons," Phys. Rev. B **43**, 9273–9274 (1991).
12. G. C. Dyer, X. Shi, B. V. Olson, S. D. Hawkins, J. F. Klem, E. A. Shaner, and W. Pan, "Far infrared edge photoresponse and persistent edge transport in an inverted InAs/GaSb heterostructure," Appl. Phys. Lett. **108**, 013106 (2016).
13. J. Wu, A. S. Mayorov, C. D. Wood, D. Mistry, L. Li, W. Muchenje, M. C. Rosamond, L. Chen, E. H. Linfield, A. G. Davies, and J. E. Cunningham, "Excitation, detection, and electrostatic manipulation of terahertz-frequency range plasmons in a two-dimensional electron system," Sci. Rep. **5**, 15420 (2015).
14. F. Stern, "Polarizability of a two-dimensional electron gas," Phys. Rev. Lett. **18**, 546–548 (1967).
15. S. J. Allen, D. C. Tsui, and R. A. Logan, "Observation of the two-dimensional plasmon in silicon inversion layers," Phys. Rev. Lett. **38**, 980–983 (1977).
16. M. Dyakonov and M. Shur, "Shallow water analogy for a ballistic field effect transistor: New mechanism of plasma wave generation by dc current," Phys. Rev. Lett. **71**, 2465–2468 (1993).

17. M. Dyakonov and M. Shur, "Detection, mixing, and frequency multiplication of terahertz radiation by two-dimensional electronic fluid," IEEE Trans. Electron Devices **43**, 380–387 (1996).
18. V. V. Popov, "The resonant terahertz response of a slot diode with a two-dimensional electron channel," Semiconductors **39**, 142–146 (2005).
19. T. Otsuji, M. Hanabe, T. Nishimura, and E. Sano, "A grating-bicoupled plasma-wave photomixer with resonant-cavity enhanced structure," Opt. Express **14**, 4815 (2006).
20. M. Dyakonov and M. S. Shur, "Current instability and plasma waves generation in ungated two-dimensional electron layers," Appl. Phys. Lett. **87**, 111501 (2005).
21. D. Hofstetter, L. Diehl, J. Faist, W. J. Schaff, J. Hwang, L. F. Eastman, and C. Zellweger, "Midinfrared intersubband absorption on AlGaN/GaN-based high-electron-mobility transistors," Appl. Phys. Lett. **80**, 2991–2993 (2002).
22. A. E. Fatimy, N. Dyakonova, Y. Meziani, T. Otsuji, W. Knap, S. Vandenbrouk, K. Madjour, D. Théron, C. Gaquiere, M. A. Poisson, S. Delage, P. Prystawko, and C. Skierbiszewski, "AlGaN/GaN high electron mobility transistors as a voltage-tunable room temperature terahertz sources," J. Appl. Phys. **107**, 024504 (2010).
23. S. Rabbaa and J. Stiens, "Charge density and plasmon modes in a triangular quantum well model for doped and undoped gated AlGaN/GaN HEMTs," J. Phys. D: Appl. Phys. **44**, 325103 (2011).
24. R. Kastner, E. Heyman, and A. Sabban, "Spectral domain iterative analysis of single- and double-layered microstrip antennas using the conjugate gradient algorithm," IEEE Trans. Antennas Propag. **36**, 1204–1212 (1988).
25. K. A. Michalski, "Electromagnetic field computation in planar multilayers," in "Encyclopedia of RF and Microwave Engineering," (John Wiley & Sons, Inc., 2005).
26. P. J. Burke, I. B. Spielman, J. P. Eisenstein, L. N. Pfeiffer, and K. W. West, "High frequency conductivity of the high-mobility two-dimensional electron gas," Appl. Phys. Lett. **76**, 745–747 (2000).
27. J. S. Gómez-díaz and J. Perruisseau-carrier, "Propagation of hybrid transverse magnetic-transverse electric plasmons on magnetically biased graphene sheets," J. Appl. Phys. **112**, 124906 (2012).
28. W. H. Press, S. A. Teukolsky, W. T. Vetterling, and B. P. Flannery, *Numerical Recipes* (Cambridge University Pr., 2007).
29. M. Nakayama, "Theory of surface waves coupled to surface carriers," J. Phys. Soc. Jpn. **36**, 393–398 (1974).
30. A. Eguiluz, T. K. Lee, J. J. Quinn, and K. W. Chiu, "Interface excitations in metal-insulator-semiconductor structures," Phys. Rev. B **11**, 4989–4993 (1975).
31. A. V. Muravjov, D. B. Veksler, V. V. Popov, O. V. Polischuk, N. Pala, X. Hu, R. Gaska, H. Saxena, R. E. Peale, and M. S. Shur, "Temperature dependence of plasmonic terahertz absorption in grating-gate gallium-nitride transistor structures," Appl. Phys. Lett. **96**, 042105 (2010).
32. V. V. Popov, A. N. Koudymov, M. Shur, and O. V. Polischuk, "Tuning of ungated plasmons by a gate in the field-effect transistor with two-dimensional electron channel," J. Appl. Phys. **104**, 024508 (2008).
33. T. Ando, A. B. Fowler, and F. Stern, "Electronic properties of two-dimensional systems," Rev. Mod. Phys. **54**, 437–672 (1982).
34. V. V. Popov, M. S. Shur, G. M. Tsymbalov, and D. V. Fateev, "Higher-order plasmon reson in GaN-based field-effect transistor arrays," Int. J. High Speed Electron. Syst. **17**, 557–566 (2007).

1. Introduction

In conventional wide-field fluorescent microscopy, a sample is uniformly illuminated by a beam of light, and the resulting fluorescence is observed in the far-field through the objective lens. The uniform intensity of the illumination along the sample fundamentally restricts the resolution of the system to half the wavelength of light due to the Abbe diffraction limit. With ever growing need to image miniscule objects especially in life sciences, modern microscopy techniques such as confocal and linear structured illumination microscopy (SIM) use spatially non-uniform sources of light to illuminate the sample. This non-uniformity is directly attributed to obtaining resolution that can be extended beyond the diffraction limit by a factor of 2 [1, 2]. Use of pinholes in confocal microscopy makes the technique highly inefficient as a significant part of light is discarded that may leave weakly fluorescent objects undetectable. Structured Illumination microscopy is a wide-field technique in which a fine illumination pattern such as a sinusoidal standing wave is used to generate *Moiré fringes* in the observed image [3, 4]. The high frequency content is mathematically reconstructed from a series of images acquired by shifting the pattern. Using a non-linear version of SIM, theoretically unlimited resolution can be achieved [5]. However, high levels of illumination intensity are required, subjecting the sample to significant damage due to thermal effects.

Resolution beyond the classical diffraction by a factor greater than 2 can be realized when an object is illuminated by surface waves, that are electromagnetic waves found at a material

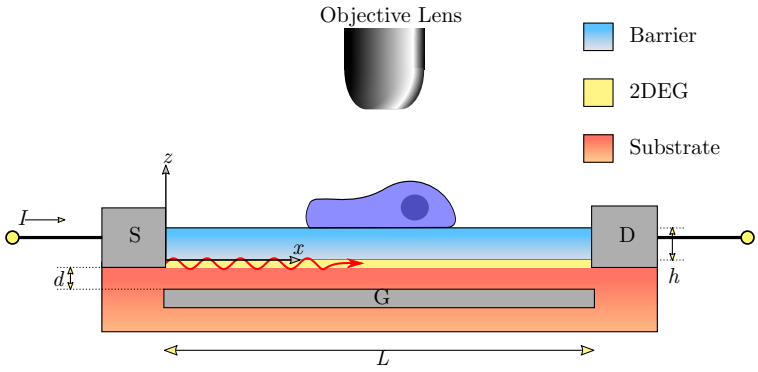

Fig. 1: Illustration of the imaging scheme where sample is excited by plasma wave pattern generated underneath by a current-driven instability

interface where one of the media possesses a complex dielectric function with a negative real part. The wavelength and phase velocity of the surface waves are much smaller than the homogeneous waves at the same frequency in a given medium. Using a grating structure to generate the surface waves with sub-diffraction features, a resolution with magnification factor of 20 was first demonstrated at optical frequencies by Nassenstein [6]. Recently, a plasmonic structured illumination microscopy (PSIM) technique was proposed in which a sample was excited by surface plasmons existing at a metal-dielectric interface in the optical frequency range [7]. In another scheme, it was shown that a hundred-fold resolution enhancement is possible using mid-infrared graphene plasmons [8, 9].

Current-drive plasma instabilities have mainly been studied in the context of ionized gases [10]. An analogous activity leads to generation of plasma waves in solid-state devices [11] that has led to many interesting applications in the far-infrared frequency region [12, 13]. A two-dimensional electron gas (2DEG) is formed at the interface of epitaxially grown semiconductors that acts as a transistor channel. In addition to the unusually high electron mobility, free-electron densities comparable to metals are observed without any intentional doping in the channel. Plasma waves originating in the field-effect transistor electron channel, which is only a few atoms thick, were discovered more than 40 years ago [14, 15] when an external TM polarized plane wave was used to excite the channel. Field-effect transistor plasma waves have lately received great interest because of their application in engineering terahertz frequency sources and sensors [16–20]. Although research has mainly been focused in realizing far-infrared devices, nitride based heterostructures have been used for the mid-infrared frequencies [21]. More importantly, the frequency response of the device can be tuned by varying the gate voltage [22, 23].

In this paper, a nanoscale imaging technique is presented in which subwavelength plasma waves, generated by a current in a transistor channel that can be tuned by controlling gate voltage, are used as the illumination pattern required for SIM. The configuration effectively creates a much larger observable spatial frequency region as compared to a far-infrared (terahertz) plane wave. Due to the linear nature of the scheme, resolution of up to two orders of magnitude beyond the diffraction limit can be obtained with a weak field intensity. Although the wavelength is very small along the channel, it simultaneously brings the disadvantage of a fast decay in the vertical direction. The presence of a semiconductor layer above the channel further reduces the intensity of the wave. The resolution enhancement is ultimately limited by the layer thickness which should be kept as small as the fabrication process permits in order to reduce attenuation of the standing wave in the vertical direction.

2. Theory

2.1. Dispersion relation

A schematic diagram of the proposed system which is similar to a transistor, is shown in Fig. 1 where a 2DEG that acts as a transistor channel is formed at the interface of two semiconductor materials of slightly different band-gap energies. Plasma waves are generated in the channel when the source and drain terminals are driven by a current source. Due to reflections from the conducting boundaries, the channel region forms a cavity in which the plasma waves form a standing wave. The structure is backed by a gate terminal that spans the length L of the channel and spaced a distance d below the 2DEG. The gate capacitively couples with the 2DEG, and by varying the voltage, the velocity as well as concentration of electrons in the channel can be controlled. A barrier layer of thickness h separates the sample from the 2DEG.

The compressed nature of the plasma waves can be described by its dispersion relation. Here, we consider the sample stage which is terminated by a gate at the bottom and free-space at the top, excited by a TM polarized plane wave. The effects of the drain and source terminals are ignored by assuming the layered semiconductor structure along with the 2DEG channel to be of infinite lateral extent. The dispersion relation which shows a frequency dependent resonance response of plasma waves in the 2D channel, is obtained by imposing the transverse resonance condition realized by an equivalent transmission line (TL) circuit [24,25]. The 2DEG is modeled as a shunt admittance related to Drude-type surface conductivity [26],

$$Y_\sigma = \sigma_s = \frac{N_s e^2 \tau}{m^*} \frac{1}{1 + \mathrm{j}\omega\tau}, \tag{1}$$

where N_s is the surface electron density in the channel, e is the electron charge, m^* is the effective electron mass in the heterostructure, τ is the scattering time of electrons, and ω is the angular frequency. The dispersion relation is then written as [27]:

$$Y^{\uparrow}(z_0) + Y^{\downarrow}(z_0) + Y_\sigma = 0. \tag{2}$$

Here, $Y^{\uparrow}(z_0)$ and $Y^{\downarrow}(z_0)$ are the up- and down-looking TL admittances from the 2DEG located at $z = 0$, and expressed as:

$$Y^{\uparrow}(z_0) = Y_2 \frac{1 - \Gamma^{\uparrow}(z_0)}{1 + \Gamma^{\uparrow}(z_0)}, \tag{3a}$$

$$Y^{\downarrow}(z_0) = -\mathrm{j} Y_1 \cot(k_{z1} h). \tag{3b}$$

For each layer, Y_i and k_{zi} where $i = 0, 1, 2$ are the respective TM mode admittance and transverse wavenumber of free-space, barrier and substrate layers respectively given by:

$$Y_i = \frac{\omega \varepsilon_i \varepsilon_0}{k_{zi}}, \qquad k_{zi} = \pm\sqrt{k_0^2 \varepsilon_i - k_x^2} \tag{4}$$

where ε_i is the relative permittivity of i^{th} layer and k_x is the longitudinal propagation constant of the structure. The upward-looking reflection coefficient $\Gamma^{\uparrow}$ in (3a) is expressed in terms of the TM mode admittances:

$$\Gamma^{\uparrow}(z_0) = \frac{Y_1 - Y_0}{Y_0 + Y_1} \exp(-2\mathrm{j} k_{z2} d_1) \tag{5}$$

A closed-form expression for the longitudinal propagation constant k_x determined by solving (2) is tedious, therefore numerical root-finding techniques such as the Newton method [28] have to be employed. As an example, the dispersion diagram of a AlGaN/GaN heterostructure is shown in Fig. 2a with no gate bias applied along with a light line whose slope is multiplied by a factor

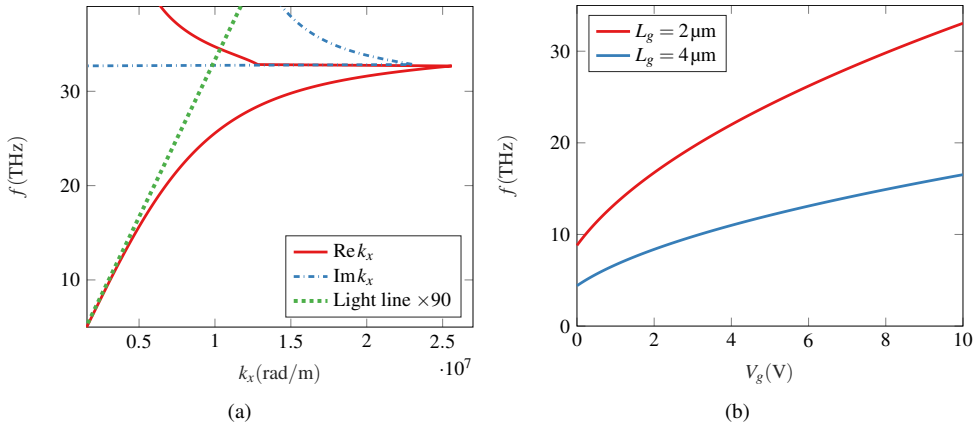

Fig. 2: (a) Plasma wave Dispersion diagram for a transistor structure supporting a 2DEG channel. (b) Effect of gate voltage on resonant frequency

of 90 for illustration. The real part corresponds to propagation and imaginary part accounts for decay of the wave. The result is similar to the dispersion curve of gated 2DEG plasmons in which the gate terminal is located at the top [29, 30]. At 25 THz, the plasmon wavenumber is approximately 80 times greater than the free-space propagation constant for a plane wave. Furthermore, the loss which is related to the imaginary part of the plasmon wavenumber is also negligible. A sample observed through such a highly subwavelength illumination makes super-resolution possible. In Fig. 2b, control of the resonant frequency by varying the gate voltage is shown, using (6) and (7). As expected, reducing the length of the channel will increase the resonant frequency, similar to what is observed for a dipole antenna. The structure parameters used to compute the dispersion relation via (1)-(5) are now briefly discussed.

The gate-channel separation is $d = 100\,\text{nm}$. The channel length L is 2 µm whereas the AlGaN barrier layer is $h = 20\,\text{nm}$ wide. The permittivity of both semiconductor layers is approximated to the static value, i.e., $\varepsilon_1 \approx \varepsilon_2 = 9.5$. Here the mole-fraction of aluminum in AlGaN alloy is 0.2 [31]. A surface carrier density of $N_s = 5 \times 10^{13}\,\text{cm}^{-2}$ and scattering time τ of 114 ps corresponding to a temperature of 3 K is assumed. As the temperature is increased, τ gets smaller which leads to reduced mobility and introduces loss in the channel. Through the gate voltage V_g, the electron density N_s of the channel can be varied using:

$$N_s = N_0 \times \left(1 - \frac{V_g}{V_T}\right), \tag{6}$$

where N_0 is the zero-bias density and V_T is the gate threshold voltage of the transistor. For a channel terminated by highly conducting source and drain terminals at each side, the resonant frequency as a function of carrier density is expressed as [32]:

$$\omega = \sqrt{\frac{N_s e^2 d}{m_* \varepsilon}\,\frac{\pi}{L}} \tag{7}$$

where ε is the average permittivity of the surrounding media. The tunability of plasma waves obtained by using (6) and (7), and assuming a gate threshold voltage of $-0.764\,\text{V}$ is shown in Fig. 2b. As expected, increasing the length of the channel reduces the resonant frequency.

2.2. Image Reconstruction

As seen in Fig. 5a, the plasma wave illumination pattern $I(\mathbf{r})$ can be assumed sinusoidal and expressed as:

$$I(\mathbf{r}) = 1 + \cos\big(\mathbf{k}_\rho \cdot \mathbf{r} + \phi\big) \tag{8}$$

where $\mathbf{k}_\rho = k_x\hat{\mathbf{x}} + k_y\hat{\mathbf{y}}$ is the spatial frequency wavevector, $\mathbf{r} = x\hat{\mathbf{x}} + y\hat{\mathbf{y}}$ is the two-dimensional positional vector and ϕ is the pattern phase. An image $M(\mathbf{r})$ of a sample atom distribution $F(\mathbf{r})$ observed through a microscope can be expressed as:

$$M(\mathbf{r}) = [F(\mathbf{r}) \cdot I(\mathbf{r})] \otimes H(\mathbf{r}) \tag{9}$$

where $H(\mathbf{r})$ is the point spread function (PSF) of the microscope, and $\cdot, \otimes$ denote multiplication and convolution operations in the spatial domain respectively. A frequency domain representation of the image obtained by taking the Fourier transform of (9) is expressed as:

$$\begin{aligned} \tilde{M}(\mathbf{k}) &= \left[\tilde{F}(\mathbf{k}) \otimes \tilde{I}(\mathbf{k})\right] \cdot \tilde{H}(\mathbf{k}) \\ &= \frac{1}{2}\left[2\tilde{F}(\mathbf{k}) + \tilde{F}(\mathbf{k} - \mathbf{k}_\rho)\exp(-\mathrm{j}\phi) + \tilde{F}(\mathbf{k} + \mathbf{k}_\rho)\exp(\mathrm{j}\phi)\right] \cdot \tilde{H}(\mathbf{k}) \end{aligned} \tag{10}$$

where $\sim$ over the letters indicates a frequency domain term and $\tilde{H}(k)$ is the optical transfer function (OTF) of the microscope. A spatial frequency representation of the scheme is illustrated in Fig. 3. In this scheme, we assume that the numerical aperture of the objective lens is unity, in which case the OTF is described by a circular disc as shown in Fig. 3(a) where the passband is bounded by $\sqrt{k_x^2 + k_y^2} = 2k_0 = \nu$. Since the plasmon frequency falls in the mid-infrared region, a relatively small k_0 implies that we need to image the sample a large number of times, which results in a slow imaging process. The process can be expedited by using an additional illumination such as a laser with frequency ω_υ in the visible region. As shown in Fig. 4, the molecules in the sample are first excited from the ground state, $|g\rangle$ to the energy level $|e\rangle$ by using a laser of frequency ω_υ. The plasmonic pattern then excites the molecules to an additional level, $|a\rangle$. Utilizing the spontaneous decay of the molecules from $|a\rangle$, we image the sample with photons of frequency $\omega_{ac} = \omega_a - \omega_c$. Here, ω_a and ω_c are the respective frequencies of energy levels $|a\rangle$ and $|c\rangle$. A frequency-selective photonic crystal is placed behind the objective lens to filter the photons of different frequencies. As a consequence of the preceding discussion, the resulting passband in the spatial frequency is now bounded by $\sqrt{k_x^2 + k_y^2} = 2k_{ac} = 2\omega_{ac}/c = \kappa$, which is the larger circle illustrated in Fig. 3. Since the frequency κ is much larger than ω_ν, high resolution can be realized by imaging the sample only a few number of times. As evident in (10), a sinusoidal illumination pattern has three frequency components, which generate an image that is a linear combination of the sample along with two shifted versions as shown in Fig. 3b. To reconstruct the sample, three different images need to be captured with each possessing a different phase term ϕ. The process can be expressed as a system of linear equations,

$$\tilde{H}(\mathbf{k}) \cdot \begin{bmatrix} \tilde{F}(\mathbf{k}) \\ \tilde{F}(\mathbf{k} - \mathbf{k}_\rho) \\ \tilde{F}(\mathbf{k} + \mathbf{k}_\rho) \end{bmatrix} = \begin{bmatrix} 2 & \exp(-\mathrm{j}\phi_1) & \exp(\mathrm{j}\phi_1) \\ 2 & \exp(-\mathrm{j}\phi_2) & \exp(\mathrm{j}\phi_2) \\ 2 & \exp(-\mathrm{j}\phi_3) & \exp(\mathrm{j}\phi_3) \end{bmatrix}^{-1} \begin{bmatrix} \tilde{M}_1(\mathbf{k}) \\ \tilde{M}_2(\mathbf{k}) \\ \tilde{M}_3(\mathbf{k}) \end{bmatrix} \tag{11}$$

The phase shifts in (11) are known beforehand. Frequency content of the sample up to k_ρ can therefore be observed due the Moiré effect which transports the high frequency information in to the observation region. To achieve two-dimensional enhancement in resolution, either the sample must be rotated about the optical axis of the microscope or the angular distribution of the illumination needs to be varied. In order to solve the three components of the spatial frequency as shown in above equation, we need to shift the plasmonic patterns. Our simulation results show

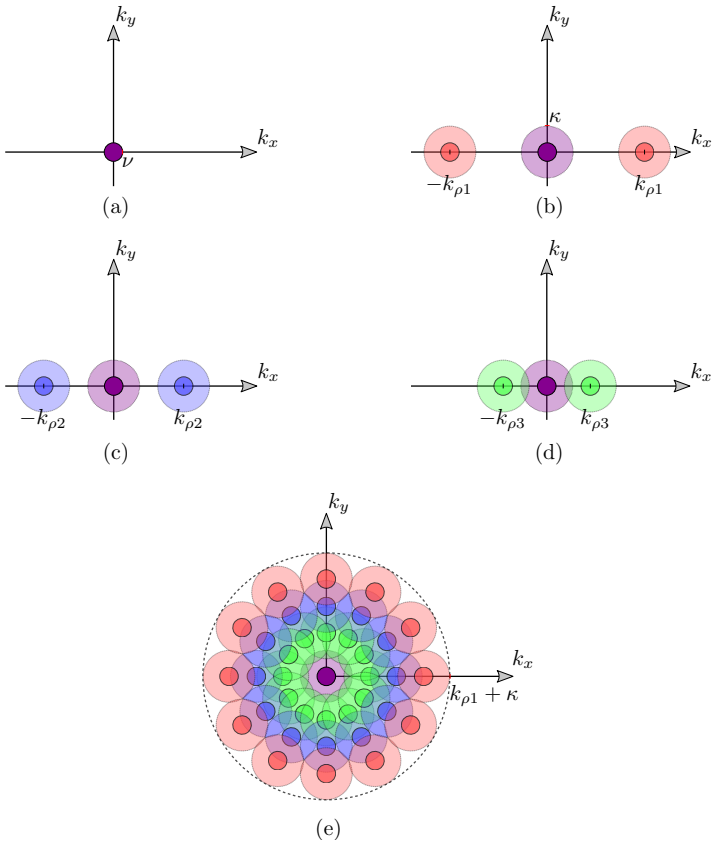

Fig. 3: Resolution enhancement through SIM: (a) Diffraction limited observable region in frequency domain. Moiré effect using a sinusoidal illumination pattern bringing high frequency content under the observable region. Sample illuminated at different plasma frequencies: (b)-(d). (e) Effective resolution enhancement of $k_{\rho1} + \kappa$ in two dimensions can be obtained after rotating the sample with respect to the optical axis

that an additional incident plane wave can shift the pattern efficiently and the amount of shift is controlled by varying the angle of incidence with respect to the optical axis. Figure 5a shows a

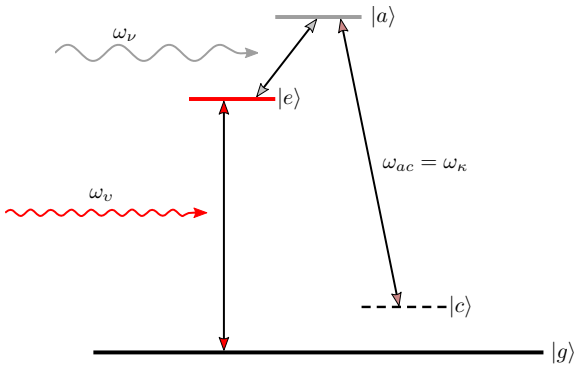

Fig. 4: Sample excited to additional energy levels to enhance the spontaneous decay, ω_κ.

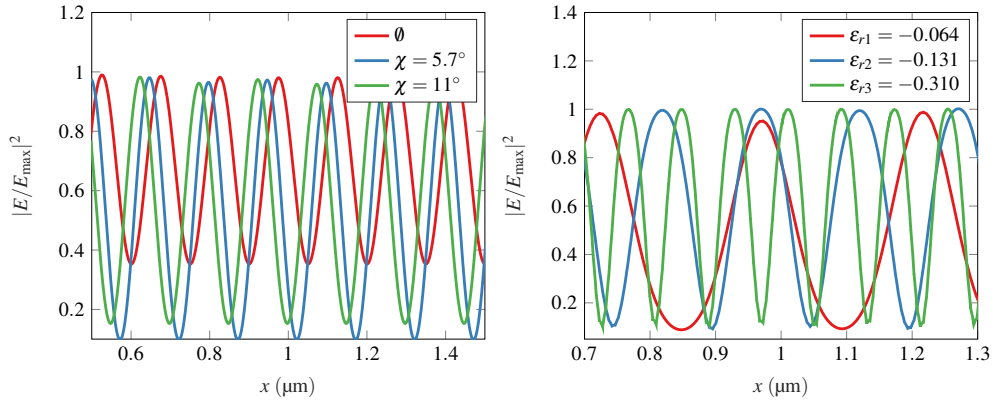

Fig. 5: Full-wave simulation results: (a) Phase shift achieved by exciting the structure with an additional illumination at an angle. (b) Tuning of the standing wave structure by applying gate bias

plot of normalized intensities. The first curve is the standing wave pattern obtained at the top surface which is only due to the surface current in the channel below. The remaining curves show the shifting of the standing wave, achieved by an additional plane wave incident from the top of the structure, whose intensity is greater than that of the plasma wave in the channel. By changing the angle of incidence slightly, different phase variations are acquired that are needed to solve the spatial frequency in (11). Only a small portion of the channel is illustrated in Figs. 5a and 5b, because the plasmonic wavelength is much smaller than the channel length L. A full-wave simulator (COMSOL) was used to plot the results. Simulated standing wave patterns tuned to different frequencies by varying the gate voltage are shown in Fig. 5b. The resulting change in electron density modifies the surface conductivity (1) of the 2DEG and the dielectric function $\varepsilon(\omega) = 1 - \mathrm{j}\sigma_s/(\omega\Delta\varepsilon_r)$ [33] where Δ is the 2DEG thickness and ε_r is the permittivity of the surrounding media.

The 2DEG channel essentially behaves as a cavity due to the resonance effects introduced by the two conducting boundaries, i.e., drain and source terminals. Therefore, the plasmon wavenumber, k_ρ can not be varied in a continuous fashion to cover all spatial frequencies. As an example, we set the length of the heterostructure and the resulting 2DEG channel to 2 μm in the simulation. Like any resonating structure, the plasmonic modes of the 2DEG channel are well-defined [31, 32, 34]. In terms of the wavenumber, the mode separation is approximately, $\Delta_k = 2\pi/(2 \times 10^{-6})$ rad/m. Thus, full coverage of all the spatial frequencies, just by tuning the plasma wave, cannot be accomplished. However, as discussed earlier, through the larger circle shown in Fig. 3, all the spatial frequencies up to the plasmon wavenumber can be recovered. For a laser having a wavelength of 600 nm, the circle radius is $\kappa = 4\pi/(6 \times 10^{-7})$ rad/m. We note that $\Delta_k \ll \kappa$, meaning that fewer images of the sample are required to realize super-resolution.

3. Simulated Results

We consider a sample with atom distribution shown in Fig. 6a. Each particle shown has a diameter of 1 nm. The minimum separation between the atoms is 38 nm and maximum is 137 nm. The 2D plasma waves are generated by a dc current-driven instability that can also be equivalently excited by a TM polarized plane wave having a frequency of 25 THz, $\hbar\omega = 0.1$ eV at zero gate bias. It is assumed that the numerical aperture (NA) is 1. To demonstrate the super-resolution

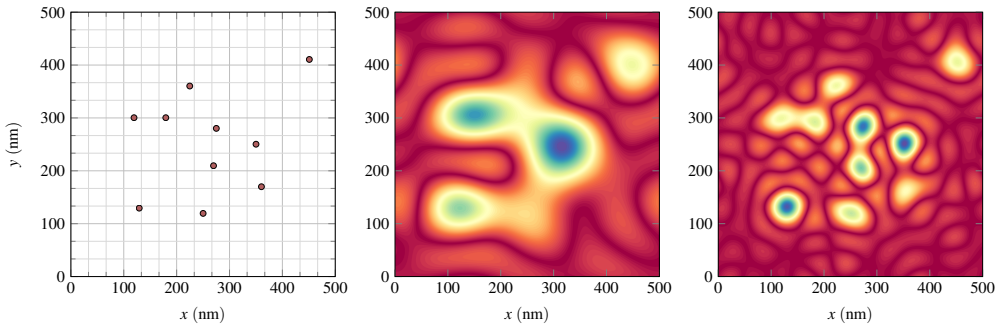

Fig. 6: (a) Sample distribution. Simulation of the reconstructed sample image at: (b) Re $k_\rho = 39.5$ (c) Re $k_\rho = 80$

technique, the atom distribution is first Fourier transformed to the spatial frequency domain. The critical step to achieve super-resolution reconstruction involves computation of the inverse Fourier transform using frequency content up to a circular region of radius $2k_\rho + \kappa$, where k_ρ can be varied by gate voltage. In Figs. 6b and 6c, a resolution enhancement 39.5 and 80 is shown corresponding to 152 nm and 74.9 nm resolution respectively. Figure. 6b shows that the particles that are separated by a distance less than the resolution can not be resolved and appear as a contiguous blurry streak, whereas they are distinguishable in Fig. 6c. The sample is imaged about 20 times, which in terms of imaging speed is very fast and can be compared with nonlinear SIM [5]. However, unlike non-linear SIM, we use a weak illumination intensity in our scheme.

In the previous simulations, we didn't consider the loss in the 2DEG channel, which can introduce irregularities in the field pattern. These irregularities result in an erroneous solution for the three frequency components in (11), which are the circular regions shown in Fig. 3b, subsequently inducing image distortion. However, with ever improving nanofabrication processing techniques, the loss along the 2DEG channel can be very small especially at low temperature, which subsequently means a large $\mathrm{Re}(k_\rho)/\mathrm{Im}(k_\rho)$ ratio. If the sample size is much smaller than the plasma wave propagation length, $1/\mathrm{Im}(k_\rho)$, the irregularities resulting from the loss can be neglected.

4. Conclusion

We propose a super-resolution nanoscopy scheme based on the subwavelength surface electromagnetic plasma found in a semiconductor heterostructure. This method is useful in particular for light-sensitive samples as it requires a weak field intensity for illumination. In comparison with the metal based SIM where the plasmonic pattern is fixed by a determined structure, we can control the period of the plasmonic pattern by varying the gate voltage. Moreover, in contrast to graphene based SIM, our scheme uses surface current to excite the plasmons, which does not require any wavenumber matching mechanism like gratings. The image reconstruction algorithm is as efficient as in conventional linear SIM, yet the high wavenumber along with the tunability of the plasma waves allows it to achieve subdiffraction resolution of up to 80 times in the mid-infrared range.

Funding

This research is supported by Qatar National Research Fund (QNRF) under National Priorities Research Program (NPRP) Grant No. 8-352-1-074.